RSC Advances

ROYAL SOCIETY OF CHEMISTRY

www.rsc.org/advances

Fabricating Novel Porous Releaser of Heparin

M.M. Wan, H.Y. Zhu, W.J. Qian, S.Q. Tao, Y. Wang, J.H. Zhu

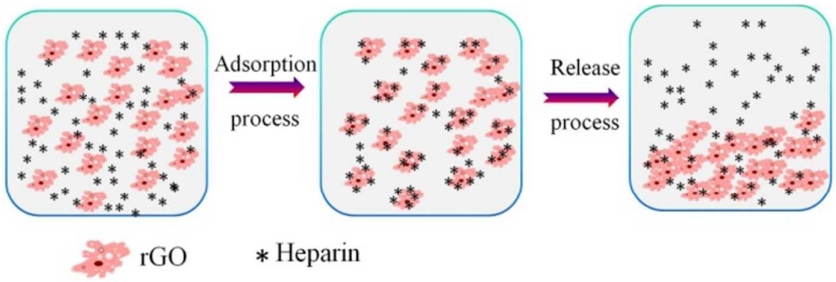

Reduced graphene oxide (rGO) could adsorb heparin of 112 mg g^{-1} and released 80% of them within 30 days.

Cite this: DOI: 10.1039/c0xx00000x

www.rsc.org/xxxxxx

ARTICLE TYPE

Fabricating Novel Porous Releaser of Heparin

Mi Mi Wan,[a] Hao Yue Zhu,[b] Wen Juan Qian,[a] Si Qi Tao,[c] Ying Wang*[c] and Jian Hua Zhu*[a]

Received (in XXX, XXX) Xth XXXXXXXXX 20XX, Accepted Xth XXXXXXXXX 20XX
DOI: 10.1039/b000000x

An achievement of increasing the both adsorption and release of heparin in drug delivery system is reported. The reduced graphene oxide (rGO) material can efficiently adsorb heparin in aqueous solution up to 112 mg g^{-1} owing to its layered and stacked structure. Moreover, this carbon vessel is able to release 90 mg g^{-1} of the drug within 30 days, exhibiting the highest released/adsorbed ratio of 80% up to date and has become a promising candidate as a novel drug releaser.

1 Introduction

Drug release is one of the potential applications of porous functional materials in the field of life science, and one example is the release of heparin. Heparin is a highly sulphated linear polysaccharide that is often used as a powerful anticoagulant to prevent venous thrombosis among high-risk patients owing to its foreseeable anticoagulant doses [1, 2]. This drug can be introduced by injection or heparinization of blood-contacting scaffolds such as small-caliber vascular prosthesis [2-4], but the design of heparin-immobilized devices depends on several factors like pore structure, surface properties and biocompatibility of the carriers. Various heparinization methods have been studied for the drug releaser, including ion-bonding, end-point attachment and covalent-bonding techniques, while different materials such as capsule, some hydro-gels, biological or macromolecules, polymers and silica molecular sieves have been tried to be the vessel [5-8]. Recently, epitaxial growth of mesoporous silica nanoparticles on ePTFE grafts is reported [2a], in which heparin can be immobilized in the mesochannels and controllably released, fabricating a novel small-caliber vascular prosthesis (Φ < 6 mm) with long lasting antithrombogenicity and high biocompatibility. Since then the subsequent study has been focused on how to improve the adsorption and release of heparin on mesoporous silica [9-12], involving the introduction of Al, Ti or organic modifier in the vessel. Among these composites the organic modified SBA-15 could adsorb 114 mg g^{-1} of heparin and released 66% (75 mg g^{-1}) of it within 30 days [11]. However, the complex interaction between the organic groups and heparin hinders the release of the drug to some extent, therefore new effort is still required to further elevate the released/adsorbed (R/A) ratio of heparin, in order to improve the efficiency of heparin release. Indeed, this is a challenge because new vessel materials are required to optimize the guest-host interaction. Here two strategies for this aim are tried. One is the use of new non-silica carrier such as graphene oxide (GO) or mesoporous alumina, and the other is the zeolitization of mesoporous silica. GO is a rough porous carbon material with different kinds of oxygen-containing species such as epoxy, hydroxyl, carbonyl, carboxylic groups [13], and its layered and stacked structure is useful in catalyzing oxidation and hydrogen production [14-16]. GO has distinct advantages in drug delivery due to its good biocompatibility, ultrahigh drug loading capability, and the ease of surface functionalization [17, 18], but its potential application of heparin releaser has not been reported [19]. Concerning the other candidate mesoporous alumina, it is known that incorporation of Al in mesoporous silica SBA-15 can obviously improve the adsorption and release of heparin [10], and mesoporous alumina itself has exhibited some extraordinary properties in the creation of super base [20] and the orientation of basic ionic liquid [21] hence it will be assessed in terms of heparin release. Mesoporous zeolites showed an excellent performance in trapping *N*-nitrosamines due to the hierarchical porosity [22], which spurs us to thermally transform two mesoporous silica samples, MCM-41 and SBA-15 along with their Al-containing analogues to MFI type zeolite and use them for adsorption and release of heparin to explore whether such improvement will be reappeared.

2 Experimental

2.1 Material preparation

Reduced graphene oxide (rGO) sample was prepared using a modified Hummers' method [23]. In a typical procedure, 3 g of graphite, 3 g of $NaNO_3$ and 66 mL of concentrated H_2SO_4 were added into a flask and stirred in an ice bath. Next, 12 g of $KMnO_4$ was added into the mixture gradually, and the reaction mixture was stirred at 321 K for 0.5 h, followed by the addition of 120 mL of water and stirred at 358 K. Finally, 300 mL of water and 12 mL of 30% H_2O_2 were added and the mixture was stirred at 358 K. The precipitated graphite oxide was rinsed with water and diluted HCl solution as well as ethanol in sequence, then stirred in water and dried at 333 K. 180 mg of graphite oxide powder was irradiated with the microwave in the flow of nitrogen, yielding to the sample denoted as rGO.

Mesoporous alumina was prepared as reported elsewhere [20]. 0.1 mole of $Al(NO_3)_3 \cdot 9H_2O$ was dissolved in 17.0 g of water before blended with 6.38 g of triblock copolymer P123 ($EO_{20}PO_{70}EO_{20}$), and the mixture was stirred and aged statically

at 313 K. Then the pH value of solution was adjusted to 9 by adding dropwise ammonia solution under slow stirring, followed by thermal treatment at 373 K. The obtained solid was filtered, washed, dried and then extracted with ethanol to give the sample of MA.

The fabrication of MCM-41 and its Al-containing analogues was performed according to literature [24], while the enlarged-pore MCM-41 was synthesized with the additive of decane [9]. To prepare mesoporous zeolite, TPAOH (tetra-*n*-propylammonium hydroxide) was directly introduced into the as-synthesized samples and transforming the amorphous silica wall into crystal zeolite by dry-gel conversion [22], yielding to siliceous sample named as MS-1, which was derived from MCM-41, and MS-2 from enlarged pore MCM-41, as well as MFI-type zeolite MZ1 and MZ2 from Al-containing MCM-41 (Table 1). Similarly, mesoporous silica SBA-15 and Al-containing SBA-15 samples were hydrothermally synthesized [25], and then transferred to mesoporous zeolite sample of SS and SZ1 and SZ2 (Table 1), respectively, by dry-gel conversion [22].

2.2 Characterizations

X-ray diffraction (XRD) patterns of samples were recorded on an ARL XTRA diffractometer (power 40 kV, 40 mA) using Cu-Kα radiation [2a]. N_2 adsorption-desorption isotherms were measured on a Micromeritics ASAP 2020 system at 77 K, and the sample was evacuated at 573 K prior to test. The Brunauer-Emmett-Teller (BET) specific surface area was calculated using adsorption data in the relative pressure range from 0.05 to 0.22, and the total pore volume of sample was determined from the amount adsorbed at a relative pressure of 0.99 [9], while the pore size distribution curves were calculated from the analysis of the adsorption branch of the isotherm using the improved Kruk-Jaroniec-Sayari (KJS) method [26]. The morphology of sample was observed by scanning electron microscopy (SEM) using a Hitachi S4800 FE-SEM system with 10 kV accelerating voltage and 10 mA of beam current, while TEM analysis was carried out on a JEM-1011 electron microscope operating at 200 kV. The FTIR spectra were recorded on a NEXUS870 spectrometer, and the sample was mixed with KBr [27].

2.3 Adsorption and release of heparin

To perform the adsorption of heparin [4, 9], 100 mg of powder-like sample was added into a tube containing 5 mL of PBS solution with 50 mg of heparin, and then the tube was kept in the fridge at 277 K for 72 h. After the sample was washed with 10 mL of PBS solution for three times, it was put into another 10 mL of PBS solution to assess the release of heparin, and the released amount of heparin at different time was determined by toluidine blue method [28]. For the adsorption of heparin in dilute solution [10], 50 mg of sorbent powder sample was added into a tube containing 5 mL of PBS solution with 0.3 mg mL^{-1} heparin, as mentioned above.

To study the models of heparin release, the experimental profiles of heparin release from samples were fitted to theoretical models. Higuchi (1961) model [29], $Mt/M = a\ t^{1/2}$, and Peppas (1987) models [30], $Mt/M = a\ t^{b}$, were used to investigate release mechanisms. In Higuchi formula, "a" is a constant, and M_t and M_∞ are cumulative release amounts at time t and at infinite time, respectively. For Peppas semi-empirical equation, "a" is the kinetic constant and "b" is an exponent identifying the diffusion mechanism.

In order to examine the percent hemolysis of rGO adsorbed heparin, the specimen was put into 10 mL of saline (0.9% w/v NaCl) to form sample A1, while A2 and A3 were distilled water and saline, respectively. They were statically equilibrated at 310 K for 0.5 h, and 0.2 mL of dilute blood was added and statically incubated at 310 K for 1 h. After these samples were centrifuged (2500 rpm) for 5 min, the supernatant solution was detected at 545 nm in a UV/VIS 3600 spectrophotometer and the percentage hemolysis was calculated as: $(A1 - A3)/(A2 - A3) *100\%$.

3 Results

3.1 Characterization of porous composites

Figure 1a illustrates the XRD patterns of rGO sample. Oxidation of graphite usually expands the interlayer spacing between graphene sheets and causes the emergence of peaks with 2θ near 10° at the expense of sharp graphite peak at 26.3° [16b], so the GO precursor showed a sharp (002) peak at 9.7°, indicating interlayer distances of 0.91 nm, along with the impaired peak at 26.4°. The microwave irradiation in the preparation of r-GO sample obviously weakened the peak at 9.7° and leaded to the emergence of wide peak with 2θ around 24.6°, similar to the report of TRG (thermally reduced graphene oxide, [31]). Judged from the intensity change of (002) peak, it appears that about 84% of GO is reduced. According to the SEM image presented in Fig. 2a, this rGO sample contained numerous ultrathin sheets and these sheets

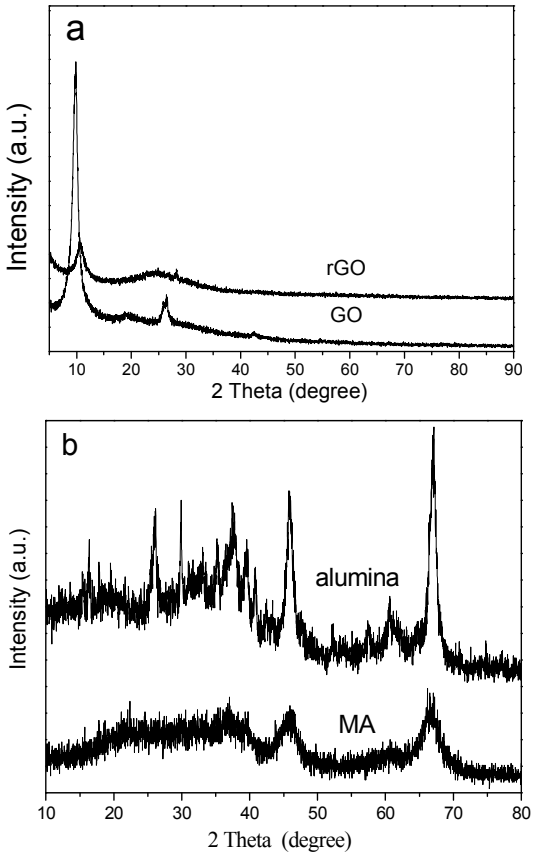

Figure 1. Wide-angle XRD patterns of (a) reduced graphene oxide (rGO) and (b) mesoporous alumina (MA).

Cite this: DOI: 10.1039/c0xx00000x

www.rsc.org/xxxxxx

ARTICLE TYPE

Table 1. Textural properties and heparin release ability of samples [a]

Samples	Si/Al ratio	S_{BET} ($m^2 \cdot g^{-1}$)	S_{mic} ($m^2 \cdot g^{-1}$)	V_p ($cm^3 \cdot g^{-1}$)	V_{mic} ($cm^3 \cdot g^{-1}$)	D_{BJH} (nm)	Adsorbed hep ($mg \cdot g^{-1}$, a)	Released hep ($mg \cdot g^{-1}$, b)	b/a (%)
rGO	-	327	43.4	0.99	0.02	-	112.4	90.2	80.2
AC	-	1445	1001	0.69	0.45	1.8	19	14.9	78.4
MA	-	294	11.9	0.71	0.002	10.0	65.2	18.4	28.2
alumina	-	208	-	0.39	0.002	6.2	25.4	13.9	54.3
MCM-41	-	1341	0	0.94	0	2.7	15.0	11.0	73.3
MS1	-	481	53.9	0.75	0.03	7.1	28.7	15.9	55.4
MS2	-	276	40.8	0.27	0.02	4.1	16.7	7.16	42.9
MZ1	15	555	55.3	0.85	0.03	4.2	67.6	22.6	33.4
MZ2	25	699	42.0	0.91	0.01	3.5	59.5	20.9	35.1
SBA-15	-	887	159.1	1.0	0.07	7.5	30.4	11.6	38.2
SS	-	240	89.5	0.34	0.04	-	35.7	12.7	35.6
SZ1	15	258	37.3	0.24	0.02	-	72.0	25.0	34.7
SZ2	60	472	76.1	1.0	0.04	9.3	77.4	16.0	20.7
NaZSM-5	12.5	354	-	0.11	-	0.5	10.2	7.7	75.5

[a] S_{BET}, BET surface area; S_{mic}, micropore area; V_p, total pore volume; V_{mic}, micropore volume; D_{BJH}, BJH mesopore diameter calculated from the adsorption branch; Release amount is the released heparin within 30 days.

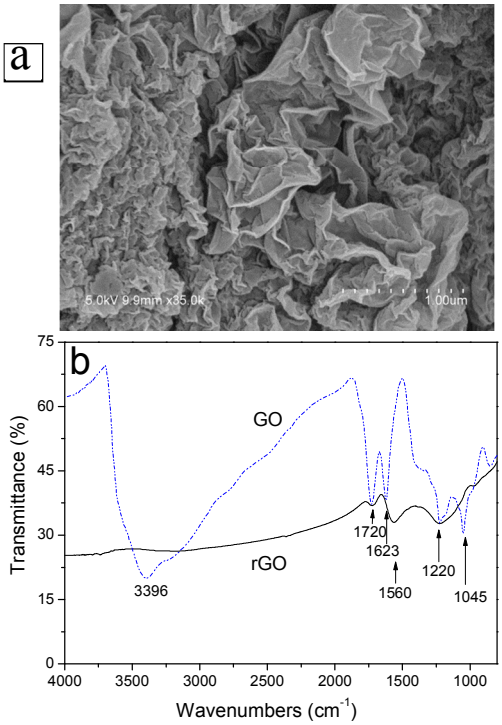

Figure 2. SEM image of rGO (a) and the FTIR spectra (b) of GO and rGO samples.

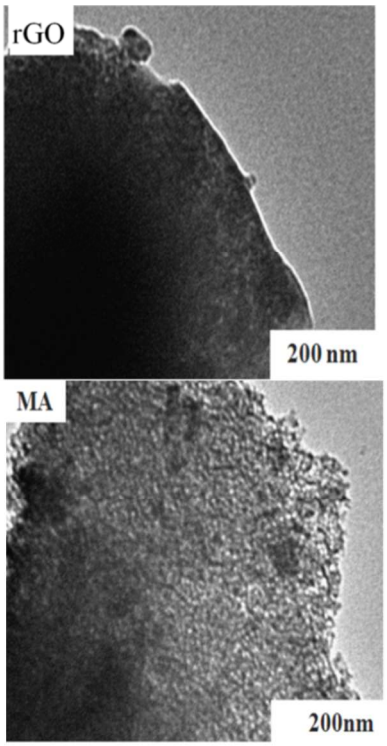

Figure 3. The TEM images of reduced grapheme oxide (rGO) and mesoporous alumina (MA) samples.

stacked randomly together to form a porous network. The stacked morphology is further verified by TEM observation in Fig. 3a, in which the superimposition of rGO sheets was obvious so that only some corrugations and pores or gapes emerged on the edge. These surface wrinkling and folding also generated lots of open edge sites that would be favorable for adsorption. As shown in Fig. 2b, GO sample had some characteristics, namely, the band around 850 cm^{-1} for the aromatic C-H deformation, 1050 cm^{-1} for C-O stretching, 1220 cm^{-1} for phenolic C-OH stretching, 1620 cm^{-1} for water H-O-H bending, and 1720 cm^{-1} for C=O stretching [32]. The broad absorption at 3000-3600 $cm^{-1}$for O-H stretching vibrations is partially related to water [32d]. In contrast, rGO sample exhibited three characteristics, 1220 cm^{-1} for phenolic C-OH stretching [32], 1560 cm^{-1} for COO^- asymmetric stretching [33], and 1720 cm^{-1} for C=O stretching [34].

Figure 1b demonstrates the XRD patterns of mesoporous alumina (MA) and γ-alumina. MA sample kept the characteristics of alumina with 2θ value of 36.9°, 46.9° and 66.8°, but their intensities were was obviously weakened [20]. The TEM image (Fig. 3b) shows the wormhole-like framework of MA. Although long-range packing order was absent, a network of channels was relatively regular in diameter, which is in agreement with the data of pore size distributions (Fig. 4b).

Figure 4 depicts the N_2 adsorption-desorption isotherms and pore size distributions of rGO and MA samples. rGO sample had the isotherm of the classical type V with an obvious H3 hysteresis loop (Fig. 4a), and its pore size distribution was quite wide, which covered the range of 2-100 nm, with a small peak appeared near 3 nm (Fig. 4b) indicating the presence of slit-like pores

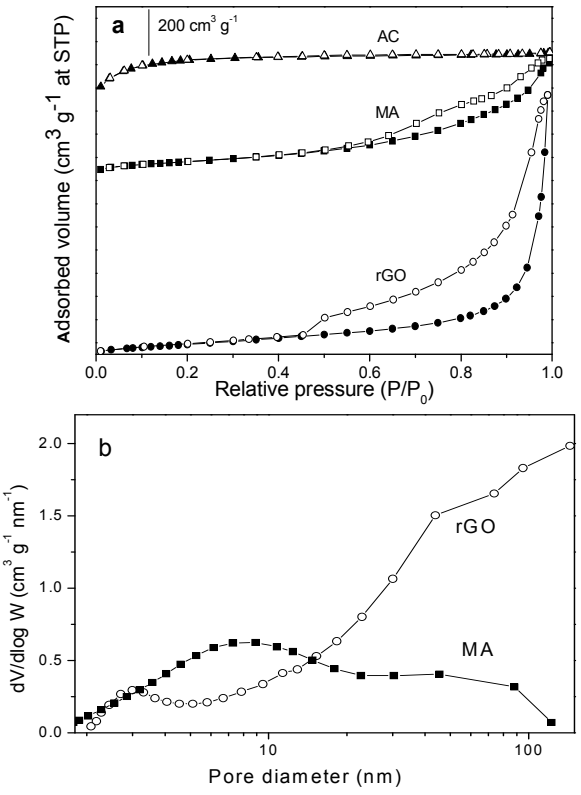

Figure 4. The N_2 adsorption–desorption isotherms (a) and pore size distribution (b) of rGO, MA and AC samples.

related to the superimposition of sheets. In contrast, AC sample had the isotherm of type I due to its microporous structure [27], and its surface area (1445 $m^2 g^{-1}$) was 3 times larger than that of rGO (327 $m^2 g^{-1}$), but the pore volume was 30% smaller (Table 1). The isotherm of MA sample was also the classical type V but its hysteresis loop was smaller than that of rGO. MA sample had a wide pore size distribution in the range of 2-100 nm and its majority was centered near 10 nm. Apart from the mesoporous structure, MA had a 40% larger surface area and 80% bigger pore volume than γ-alumina (Table 1).

Figure S1 shows the XRD patterns of the mesoporous zeolite transformed from MCM-41sample. All composites exhibited the characteristics of MFI zeolite with low intensity, but they also contained amorphous silica that formed the undulant baseline (Fig. S1a). After the steaming transformation of 12 h, MZ2 sample showed the stronger zeolitic characters than MZ1 did, owing to the higher Si/Al ratio of MZ2 sample since the aluminum in framework obstructed the zeolitization of mesoporous silica [35]. As revealed in Fig.S1b, most of the transformed samples only kept the weakened (100) peak in low-angle XRD patterns, similar to that reported on the disordered mesoporous materials such as MSU silicates [36]. Besides, the position (2θ =1.7°) on the XRD pattern of MS1 sample shifted to a lower angle compared to that of MCM-41(2θ =2.2°), mirroring the enlarged unit cell of this material. At the same time, the diffraction peaks of silicalite-1 emerged at wide-angle XRD pattern to indicate the formation of MFI structure in MS1 sample after 10 h transformation. The enlarged pore sample MS2 showed a weak structural stability because its mesoporous structure was lost in the transformation of 4 h. However, no zeolitic structure was detected on this sample (Fig. S1a).

The Al-content of mesoporous materials has a negative effect for their transformation [35]. After the conversion of 14 h, SZ2 sample still kept the mesoporous characters of SBA-15 in its XRD pattern while only (100) peak remained on that of SS1 (Fig. S1d). Such obstruction can be conquered by prolonging the steaming time. As shown in Fig. S1c, the SZ1 sample with high Al-content was considerably converted into MFI zeolite within 18 h. At the same time, this sample still kept some obvious mesoporous characters owing to the optimal transformation conditions. Similarly, SS1 sample possessed the stronger MFI zeolitic characters than that of MS1, since it underwent 14 h steaming treatment. Thermal conversion of MCM-41 leads to the emergence of H1 hysteresis loop on the N_2 adsorption-desorption isotherm, in the range of p/p_0 from 0.5 to 0.8 for MS1 and MS2 but from 0.5 to 1.0 for MZ1 and MZ2 samples (Fig. S2a). Also, their pore sizes were enlarged to some extent in comparison with those of MCM-41 (Fig. S2b). In contrast, steaming transformation of SBA-15 reduced the H1 hysteresis loop on its isotherm (Fig. S2c), and among these derivatives only SZ2 sample kept the isotherm of type IV and an obvious H1 hysteresis loop, but its p/p_0 range was shifted to higher range from 0.7 to 0.9 due to the formation of larger pores. For instance, the most probable diameter of SZ2 sample was changed from 7.5 to 9.3 nm (Fig. S2d). Also, three converted samples exhibited a smaller surface area than parent SBA-15 (Table 1), and the pore volume of SS1 and SZ1 was also considerably reduced.

3.2 Adsorption and release of heparin by porous materials

The adsorption of heparin by various porous materials is listed in Table 1. Among all the materials, rGO sample adsorbed 112 mg g^{-1} of heparin, which is about 5 times higher than AC did (19 mg g^{-1}) and is close to the highest value reported on the organic modified SBA-15 (114 mg g^{-1}, [11]). MA sample trapped 65 mg g^{-1} of the protein under the same condition, 156% more than that by γ-alumina (25 mg g^{-1}) owing to its mesoporous structure. Two mesoporous silica sorbents exhibited smaller capacities in the adsorption of heparin. MCM-41 trapped 15 mg g^{-1} and SBA-15 adsorbed 30 mg g^{-1}, which coincided with the reports in literature [9-11]. Zeolitization of MCM-41 elevated its ability so that MS1 sample could trap 90% more of the bio-molecule (Table 1). The existence of Al in mesoporous zeolite further improved the adsorption of heparin. MZ1 and MZ2 samples were able to trap the heparin of 67 and 59 mg g^{-1}, respectively. MS2 sample exhibited a weak performance in the adsorption because of its unsuccessful transformation as aforementioned. Zeolitization of SBA-15 slightly improved its adsorption capacity of heparin from 30 to 35 mg g^{-1}, but incorporation of Al in mesoporous zeolite doubled the capability so the SZ1 and SZ2 samples adsorbed the heparin over 70 mg g^{-1} (Table 1). To further examine the capability of rGO sample in adsorbing heparin, it was put into the dilute solution (0.3 mg mL^{-1}). Unlike most mesoporous sorbents which are incapable of adsorbing heparin in such solution [10, 12], rGO still adsorbed the drug of 19 mg g^{-1}.

The release of heparin from these porous sorbents is also demonstrated in Table 1. It can be seen that rGO sample was also the champion with the released amount of 90 mg g^{-1} that exceeded the highest value reported on the organic modified SBA-15 (75 mg g^{-1}, [11]). About 80% of the heparin adsorbed by rGO, denoted as the released ratio (R/A), could be released within 30 days, which is valuable for its potential application of drug releaser and seems relate to the nature of carbon material since 78% of the drug trapped by AC sample was also released (Table 1). Different situation was observed on MA composite whose released amount achieved 18 mg g^{-1} but its released ratio was only 28%, even lower than that of alumina (54%, Table 1). As a matter of fact, it is difficult to increase both the amount and ratio of heparin released. For instance, MZ1 and MZ2 samples released more heparin than MCM-41 did, however their released ratio, 33% and 35%, were lower than that of the parent (73%, Table 1). Similarly, mesoporous zeolite SZ1 released 115% more heparin than SBA-15 did, but its released ratio (34%) was 10% smaller than that of the mesoporous silica (38%). Likewise, SZ2 and SS1 samples showed a relatively low released ratio (Table 1) though they could release the heparin not less than SBA-15 did.

Figure 5a depicts the release profiles of heparin on rGO, MA, AC and alumina samples. rGO sample exhibited a significant

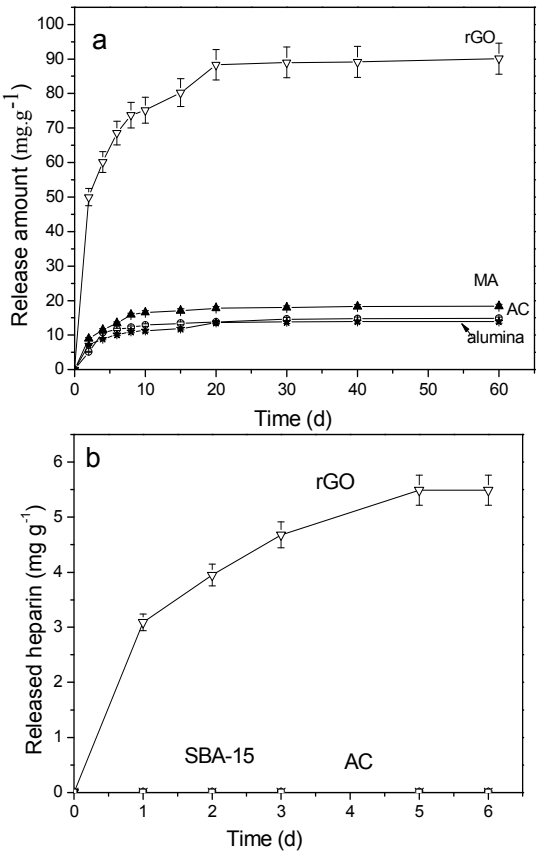

Figure 5. Release profiles of heparin on (a) reduced graphene oxide (rGO) and mesoporous alumina (MA) samples, and (b) rGO and AC as well as SBA-15 adsorbed heparin in dilute solution (0.3 mg mL^{-1}).

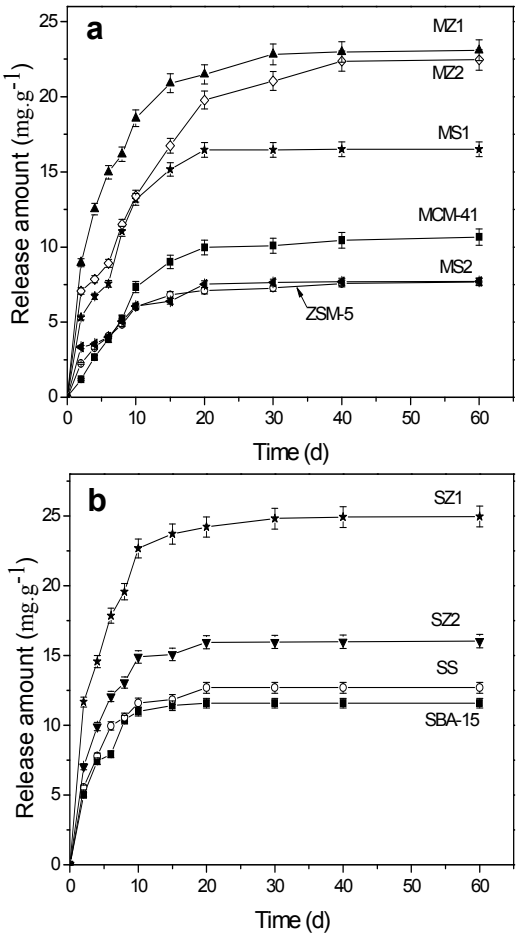

Figure 6. Release profiles of heparin on mesoporous-zeolite of (a) M and (b) S series samples.

"burst effect" owing to the desorption of the heparin located on the external surface or near the orifices in the host [37], and its released amount at the 2nd day reached 50 mg g^{-1}, 6 times more than that by AC (7 mg g^{-1}). Also, rGO released more heparin than AC did within 3 weeks and its release reached the equilibrium in 20th day, ten days longer than AC did. The amount of heparin released from rGO sample achieved 68, 75 and 88 mg g^{-1} at the 6th, 10th and 20th day, 5~6 times more than that from AC. Finally, 90 mg g^{-1} of heparin was released from rGO vehicle within 60 days, which exceeded the record of mesoporous materials up to date [11]. However, MA sample did not show an obvious elevated heparin release performance in comparison to alumina. Their release profiles seemed similar and almost parallel as shown in Figure 5a. MA sample released 25~55% more heparin than alumina did, but the absolute amount was minor (2~5 mg g^{-1}). Figure 5b illustrates the profile of heparin released from the rGO sample adsorbed the drug in dilute solution, in which about 5.5 mg g^{-1} of heparin was evenly released within 5 days and the equilibrium was achieved at 6th day. However, AC sample failed to release any the drug under the same condition (Fig. 5b).

Figure 6 illustrates how the zeolitization of mesoporous silica promotes the heparin release. MCM-41 could release about 57% more heparin than zeolite NaZSM-5 did, and they needed 30 days to reach the equilibrium (Fig. 6a). The zeolitization of MCM-41 made MS1 sample to release more heparin (~45%) within 20 days, and caused a dramatic improvement on MZ2 composite whose released amount (~21 mg g^{-1}) was 90% larger, owing to its hierarchical structure (Fig. S1a). Moreover, this vessel could keep the heparin release till the 40th day, which was precious for medicine [2a]. Similar promotion was also observed on the heparin release on mesoporous zeolite MZ1 where 22 mg g^{-1} of heparin was released within 30 days, 100% higher than that on parent MCM-41. MS2 sample is an exception whose release capability was close to that of zeolite NaZSM-5 due to its ineffectual transformation (Fig. S1a). On the other hand, the zeolitization of SBA-15 only slightly improved the heparin release on SS1 sample, but 40% enlarged the released amount (16 mg g^{-1}) on SZ2 vessel. The obvious promoted heparin release was observed on SZ1 sample where the doubled amount of heparin (25 mg g^{-1}) was released within 30 days (Fig. 6b) though a "burst effect" appeared on its release profile.

The release profiles of heparin from several samples such as MCM-41, MZ1, SBA-15 and SZ1 along with rGO are fitted to theoretical models such as Higuchi model [29] and Peppas model [30] in order to study the models of heparin release. Both models are short time approximations and limited to be applied to the first 60% of the release [9, 10]. As a consequence, the release profiles in 10 days are fitted with these two models, and the fitted results are shown in Table S1 meanwhile Figure S3 presents the fitted curves. Most of R^2 values were above 0.969, indicating the good fitting and relative correlation. The "b" value of SBA-15 and MZ1 sample was close to 0.5 (Table S1) so that their release mechanism was similar to Higuchi model, which indicates the uniform pore of the sample. Peppas model seems more suitable for fitting other samples' release profiles, and this phenomenon implies the existence of a little bit heterogeneous pores on these samples [38]. On the other hand, the hemolysis ratio of heparin-immobilized r-GO sample was 3.4%, which is lower than that of expanded polytetrafluoroethylene (ePTFE) vessel (4.7%) and the permissible hemolysis level (5%) [2a]. The adsorbed heparin considerably enhanced the biocompatibility of rGO and enabled it to be the potential biomaterial.

4 Discussion

Three factors enabled the sample of rGO to be the novel releaser of heparin. The first factor is the nature of carbon material that makes it easy to release heparin. As demonstrated in Table 1, common AC sample released 78% of the heparin adsorbed (19 mg g^{-1}), and this ratio is close to that of rGO (80%), mirroring the weak interaction between the vessel and the protein. It is such proper interaction that empowers the rGO sample to release a detectable amount of heparin even though the vessel adsorbed the drug in a diluted solution (Fig. 5b). Another factor is the specific morphology of rGO that is consisted of porous network stacked by numerous ultrathin sheets (Fig. 2a). Heparin has a special long chain structure feature of 1-1.5 nm in width, several dozens of nanometres in length [10] hence it should be a slow procedure for the chain-like heparin to diffuse inwards the porous vessel. Such randomly stacked sheets possess lots of different deep gaps or cracks, and they have relatively wide openings which are favorable for the adsorption and desorption of heparin (Scheme 1), like the fish easily enter into and leave from coral reef. In contrast, the channel of mesoporous alumina or

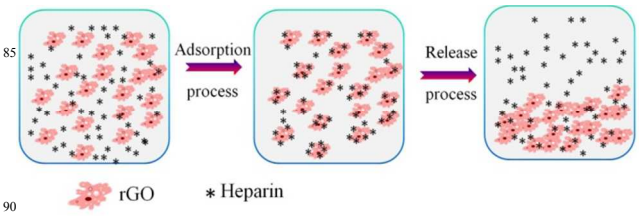

Scheme 1. Schemetic illustration of the adsorption and release process of heparin on rGO sample.

zeolites unavoidably hinders the diffusion of heparin to some extent. The third factor is the excellent hydrophilicity of rGO, which enables the sorbent to be suspended in the aqueous solution. Thus, rGO sorbent can extensively contact with heparin in solution to accommodate the guest in gallery and achieves a high loading capacity (Table 1), which ensures the succeeding release because the release of heparin from vessel into medium solution is driven by their concentration difference [9-12]. Once the heparin solution is replaced by blank solution in the release process, the loaded heparin will escape out of the gallery, forming a continual release for several weeks after the initial diffusion controlled release (Fig. 5a). Unlike mesoporous silica with a poor hydrothermal stability [39], the specific rough layered and stacked structure of GO is stable in long-term release, which avoids the retention of heparin caused by vessel structural collapse and ensures the leave of heparin from vessel, achieving the record of 90 mg g^{-1}.

Zeolitization of mesoporous silica such as MCM-41 or SBA-15 and its Al-containing analogues can considerably elevate their adsorption capacity of heparin and release capability (Table 1), because the existence of micropores in the channel wall of vessel may provide the strengthened van der Waals force for the

adsorbate and prolong the release of heparin. However, it fails to increase the released ratio of heparin, even on those Al-containing analogues. Similar situation is found on mesoporous alumina (MA) where only the adsorption of heparin was promoted. Further investigation is required to conquer this problem.

5 Conclusion

In summary, we discovered the new application of reduced graphene oxide in drug release. This carbon material can efficiently trap heparin in aqueous solution up to 112 mg g^{-1} due to its specific sheets stacked structure. Besides, it released 90 mg g^{-1} of the drug within 30 days with the highest released ratio of 80% up to date, becoming a competitive candidate for novel drug releaser. Fabrication of mesopores in alumina or zeolitization of mesoporous silica also improves the adsorption of heparin on these porous vessels, but is difficult to enhance their released ratio.

Notes and references

[a] *Key Laboratory of Mesoscopic Chemistry of MOE, College of Chemistry and Chemical Engineering, Nanjing University, Nanjing 210093, China, E-mail: jhzhu@ nju.edu.cn,*
[b] *Department of Chemistry, The Pennsylvania State University, University Park, Pennsylvania 16802, United States*
[c] *College of Chemistry & Chemical Engineering, Nanjing University, Nanjing 210093, China. Fax: 0086-25-83317761; Tel: 0086-25-83621219; E-mail: wangy@nju.edu.cn*

† Electronic Supplementary Information (ESI) available: XRD patterns, N_2 adsorption–desorption isotherms and pore size distribution of mesoporous-zeolite. See DOI: 10.1039/b000000x/

1 S. Sarkar, K. M. Sales, G. Hamilton and A. M. Seifalian, *J. Biomed. Mater. Res. Part B*, 2007, **82B**, 100.
2 (a) Y. Zhou, K. Li , J. Y. Yang , C. X. Guan , Y. Wang , C. J. Liu and J. H. Zhu, *Small*, 2012, **8**, 1373. (b) M. Tobu, O. Iqbal, D. Hoppensteadt, B. Neville, H. L. Messmore and J. Fareed, Clin. Appl. Thromb. *Hemost.*, 2004, **10**, 301; (c) J. I. Weitz and L. A. Linkins, *Expert Opin. Investig. Drugs,* 2007, **16,** 271; (d) J. I. Weitz, *Thromb. Res.*, 2010, **125** (suppl. 2), S30.
3 H. Wang, Z. X. Lin, X. M. Liu, S. Sheng and J. Wang, *J. Control. Release,* 2005, **105**, 120.
4 A. Karewicz, K. Zasada and K. Szxzubialka, *Int. J. Pharmaceut,* 2010, **385**, 163.
5 M. Prabaharan, and S. Gong, *Carbohydr. Polym.*, 2008, **73**, 117.
6 B. G. Trewyn, S. Giri, I. I. Slowing and V. S. Y. Lin, *Chem. Commun.*, 2007, 3236.
7 Y. F. Zhu, T. Ikoma, N. Hanagata and S. Kaskel, *Small*, 2010, **6**, 471.
8 K. K. Coti, M. E. Belowich, M. Liong, M. W. Ambrogio, Y. A. Lau, H. A. Khatib, J. I. Zink, N. M. Khashab and J. F. Stoddart, *Nanoscale,* 2009, **1**, 16.
9 M. M. Wan, J. Y. Yang, Y. Qiu, Y. Zhou, Ch. X. Guan, Q. Hou, W. G. Lin and J. H. Zhu, *ACS Appl. Mater. Inter.,* 2012, **4**, 4113.
10 M. M. Wan, W. J. Qian, W. G. Lin, Y. Zhou and J. H. Zhu, *J. Mater. Chem. B,* 2013, **1**, 3897.
11 W. J. Qian, M. M. Wan, W. G. Lin and J. H. Zhu, *J. Mater. Chem. B,* 2014, **2**, 92.
12 M. M. Wan, X. D. Sun, W. J. Qian, S. Liu, J. Ma and J. H. Zhu, *Microporous Mesoporous Mater.*, 2014, **199**, 40.
13 M. Inagaki and F. Kang, *J. Mater. Chem. A,* 2014, **2**, 13193.
14 B. Frank, R. Blume, A. Rinaldi, A. Trunschke and R. Schlögl, *Angew. Chem. Int. Ed.*, 2011, **50**, 10226.
15 D. R. Dreyer, H. P. Jia and C. W. Bielawski, *Angew. Chem. Int. Ed.,* 2010, **49**, 6813.
16 (a) T. F. Yeh, J. M. Syu, C. Cheng, T. H. Chang and H. Teng, *Adv. Funct. Mater.*, 2010, **20**, 2255. (b) T. F. Yeh, F. F. Chen, C. T. Hsieh and H. Teng, *J. Phys. Chem. C,* 2011, **115**, 22587.
17 K. Yang, L. Z. Feng, X. Z. Shi and Z. Liu, *Chem. Soc. Rev.*, 2013, **42,** 530.
18 E. Morales-Narvaez and A. Merkoci, *Adv. Mater.,* 2012, **24**, 3298.
19 T. J. Parka, Y. S. Kima, T. Hwanga, P. GOvindaiaha, S. W. Choib, E. Kima, K. Wonc, S. H. Leed and J. H. Kima, *Process Biochemistry,* 2012, **47**, 113.
20 L. B. Sun, J. Yang, J. H. Kou, F. N. Gu, Y. Chun, Y. Wang, J. H. Zhu and Z. G. Zou. *Angew. Chem. Int. Ed.,* 2008, **47**, 3418.
21 M. M. Wan, H. Y. Zhu, Y. Y. Li, J. Ma, S. Liu and J. H. Zhu, *ACS Appl. Mater. Interfaces,* 2014, **6**, 12947.
22 M. B. Yue, L. B. Sun, T. T. Zhuang, X. Dong, Y. Chun and J. H. Zhu. *J. Mater. Chem.*, 2008, **18**, 2044.
23 W. S. Hummers and R. E. Offeman, J. Am. Chem. Soc. 1958, 80, 1339.
24 S. C. Shen, X. Chen and S. Kawi, *Langmuir*, 2004, **20**, 9130.
25 D. Y. Zhao, J. L. Feng, Q. S. Huo, N. Melosh, G. H. Fredrickson, B. F. Chmelka and G. D. Stucky, *Science*, 1998, **279**, 548.
26 M. Jaroniec and L. Solovyov, *Langmuir*, 2006, **22**, 6757.
27 Y. Y. Li, K. K. Han, W. G. Lin, M. M. Wan, Y. Wang and J. H. Zhu, *J. Mater. Chem. A*, 2013, **1**, 12919.
28 M. S. Ahola, E. S. Sailynoja and M. H. Raitavuo, *Biomaterials,* 2001, **22**, 2163.
29 V. Hoffart, A. Lamprecht, P. Maincent, T. Lecompte, C. Vigneron and N. Ubrich, *J. Controlled Release,* 2006, **113**, 38.
30 E. Rechavia, F. Litvack, M. C. Fishbien, M. Nakamura, and N. Eigler, *Cathet. Cardiovasc. Diagn.*, 1998, **45**, 202.
31 R. Li, Z. Wei, X. Gou and W. Xu, *RSC Adv*., 2013, **3**, 9978.
32 (a) H. Suzuki, Y. Hirano, Y. Kimura, S. Takaichi, M. Kobayashi, K. Miki and Z. Y. Wang, *Biochim. Biophys. Acta,* 2007, **1767**, 1057; (b) K. A. Trick and T. E. Saliba, *Carbon,* 1995, **33**, 1509; (c) C. H. Lucas, A. J. Lopez-Peinado, J. de D. Lopez-Gonzalez, M. L. Rojas-Cervantes and R. M. Martin-Aranda, *Carbon*, 1995, **33**, 1585; (d) J. I. Paredes, S. Villar-Rodil, Martıinez-Alonso and J. M. D. Tascon, *Langmuir*, 2008, **24**, 10560.
33 Y. Li, Y. Kimura, T. Arikawa, Z. Y. Wang-Otomo and T. Ohno. *Biochemistry,* 2013, **52**, 9001.
34 H. Suzuki, M. Sugiura and T. Noguchi, *Biochemistry,* 2008, **47**, 11024.
35 J. C. Groen, J. A. Moulijna and J. Pérez-Ramírez, *J. Mater. Chem*., 2006, **16**, 2121.
36 S. S. Kim, W. Z. Zhang and T. J. Pinnavaia, *Science,* 1998, **282**, 1302.
37 L. X. Wen, Z. Z. Li, H. K. Zou, A. Q. Liu and J. F. Chen, *Pest Manag Sci.*, 2005, **61**, 583.
38 H. Ritter and D. J. Brühwiler, *J. Phys. Chem. C,* 2009, **113,** 10667.
39 R. Mokaya and W. Jones, *Chem Commun.*, 1998, **17**, 1839.